Effects of Plasma Chamber Pressure on the Etching of Micro Structures in SiO_2 With the Charging Effects

Hye Sang Park, Sung Jin Kim, Yan Qing Wu, and Jae Koo Lee, *Member, IEEE*

***Abstract*—Many problems in ion-enhanced etching are caused by the charge-up effect as the aspect ratio increases with the decrease of a semiconductor device size. The energy and angle distribution of particles are important factors in the etching process which can be controlled by the pressure of a plasma chamber. In the present paper, we varied the pressure of plasma and studied the charge-up phenomenon for the aspect ratios 5 and 10. In the low pressure RF-capacitively coupled plasma (CCP) chamber, ions with higher energy and small angle distribution have been detected. On the other hand, in the high-pressure RF-CCP chamber, ions with low-energy and high-angle distribution are observed. At a high-aspect ratio, the charge-up potential is reduced when the pressure of a plasma chamber is high. At a high pressure, more vertical etching feature is expected.**

***Index Terms*—Capacitively coupled plasma, charge-up simulation, plasma process induced damage.**

I. Introduction

ION-ENHANCED plasma etching has been widely used in the semiconductor process because of its anisotropic and accurate etching profile. In general, the motion of incident ions at the wafer surface on the electrode is more directional than that of electrons. The difference causes the electron shading effect at the etched microtrench, thus generating positive potential at the deep trench bottom. This charging effect induces many serious plasma process induced damage (PPID) problems such as bowing, trenching, reactive ion etching (RIE) lag, and notching [1], [2]. The reduction in the device size and multilayer structures requires a high-aspect ratio in the SiO_2 etching. As the aspect ratio increases, the charging effect becomes more profound [3].

In the ion-enhanced plasma etching, the vertically etched profile is an important issue. Vertical etching profile is related to the direction of incident ions, and it can be implemented by the anisotropic movement of ions. The anisotropic etching profile is obtained when the incident ions are distributed within a small angle to the normal of the electrode. The isotropic etching component of the incoming ion is caused either by thermal energy or by collisions between ions and neutrals in the sheath. Since thermal energy is negligibly small (typically less than 0.1 eV) compared to the sheath-voltage drop (near 100 eV or more), collisions in the sheath are a dominant factor in etching. Since the collision probability is proportional to pressure, the low-pressure plasma is suitable for vertical etching. Many efforts have been made to sustain plasma at low pressure including high-density plasma (HDP).

Pressure is an important factor in determining the charged potential distribution at the etched microtrench and also for anisotropic etching profile. Collisional high-pressure plasma has an advantage in reducing the charge-up potential because the difference of motions is reduced between ions and electrons. However, low-pressure plasma can make more vertical etching profile than high-pressure plasma. Therefore, the role of pressure in low charge-up damage and vertical etching profile must be investigated, and the computer modeling and simulation are a useful and effective tool in increasing the general understanding of plasma processing and charge-up mechanism.

In this study, we observe the movement of ions and electrons at the electrode of RF capacitively coupled plasma (CCP) chamber by varying the gas pressure. The RF-CCP chamber is usually used as a plasma reactor for SiO_2 etching because of its high-incident ion energy, good uniformity characteristics, and cheap cost. We calculate the movement of particles in the plasma chamber by using the conventional particle-in-cell (PIC) simulator XPDC1 [4], [5]. The energy and angle distribution of incident ions and electrons at the smaller electrode are obtained by XPDC1 simulation, and these data are used as initial condition of incident particles for charging simulation. The trench potential and the movement of ions and electrons around the trench are calculated by our three-dimensional (3-D) PIC charge-up simulator. By using the 3-D code, we can estimate their influence on the etching profile.

In Section II, the 3-D PIC charge-up modeling method are presented. The RF-CCP simulation of particle movements is described in Section III. Results of charging simulation are also discussed in Section III. Finally, the conclusion is presented in Section IV.

II. Modeling of 3-D Charge-Up Simulation

In our charge-up simulation, we are interested in one or two of the repeated submicron scale trenches. The size of several trenches is in the order of a micrometer or sub-micrometer. As the size of plasma chamber is much larger (centimeters) than that of trenches, the simulation procedure is divided into two parts—the first is plasma source simulation in the RF-CCP plasma chamber and the second is the charge-up simulation of

Manuscript received October 30, 2002; revised February 12, 2003. This work was supported by the Korea Ministry of Science and Technology under the Tera-level Nano Devices Project and 21c Frontier R&D Program, and Samsung Electronics Company.

H. S. Park is with Samsung Electronics Company, Hwasung 445-701, South Korea (e-mail: hyesang.park@samsung.com).

S. J. Kim, Y. Q. Wu, and J. K. Lee are with the Department of Electronic and Electrical Engineering, Pohang University of Science and Technology, Pohang 790-784, South Korea (e-mail: jkl@postech.ac.kr).

Digital Object Identifier 10.1109/TPS.2003.815245

microtrenches [6]–[8]. Due to small size of simulation domain, the following assumptions are reasonable for the charge-up simulation.

1) Collisions in the simulation domain are neglected because mean-free path of ions and electrons (λ_i, λ_e) is much longer than the simulation domain size.
2) The probability that more than two particles exist in the simulation space at the same time is very low because the life time of ions or electrons in the simulation region is much shorter than the incident time interval. The Laplace's equation for electric field calculation has been used.
3) The potential at the top and bottom boundaries ($y = 0$, $y = y_{\max}$) are the same because the width of sheath where potential drops significantly is much longer than the length between the top and the bottom of simulation domain. The potential of top and bottom boundary is set to zero.
4) The etching time is much longer than charge-up transient time. In the high-aspect ratio etching, the average transient charge-up time before saturation of potential is nearly 1 s, and the etch ratio is a few hundreds of nanometers per second.

During the charge-up potential transient time, the etching is negligible. In the charge-up simulation, the trench structure is fixed. The following assumptions are used to simplify the simulation.

5) The dielectric structure used in simulation is a perfect insulator, the charge of an absorbed particle is fixed, and the surface current is neglected.
6) Since the same microstructures are repeated in CMOS devices, we set periodic boundary conditions. The boundary conditions are explained on the following.

The charge-up potential calculation is briefly outlined in the flow chart in Fig. 1. One computational cycle consists of three modules, particle loading, calculation of particle trajectory and calculation of potential. Ion angle energy distribution function (IAEDF) and electron angle energy distribution function (EAEDF) are obtained by RF-CCP simulation. Initial direction and energy of ions and electrons are determined by randomly sampling the IAEDF and EAEDF. As the incident ion and electron fluxes at the electrode are the same when plasma discharge approaches the saturation, incident ion and electron numbers are the same. Every 500 ion and electron superparticles are generated for one simulation cycle, and each superparticle represent 0.1 of a real particle. The reason for using many superparticles is to reduce simulation noise. As the electric field generated by one absorbed particle is very strong in the micro- or nanoscale range, the absorbed position of one particle is an important factor in determining the trajectory of the next incident particles and the potential profile. Using many particles absorbed into various regions at the same time can decrease the strong electric field generated by a single particle. The reduction of the ratio between the superparticle and a real particle also can mitigate the power of a single particle.

The simulation space is schematically shown in Fig. 2. There exist six boundary planes: the left ($x = 0$), right ($x = x_{\max}$),

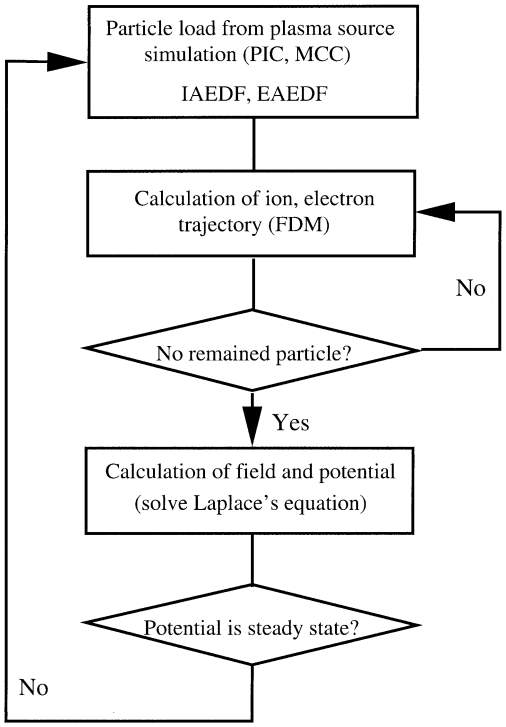

Fig. 1. Flow chart of charge-up simulation.

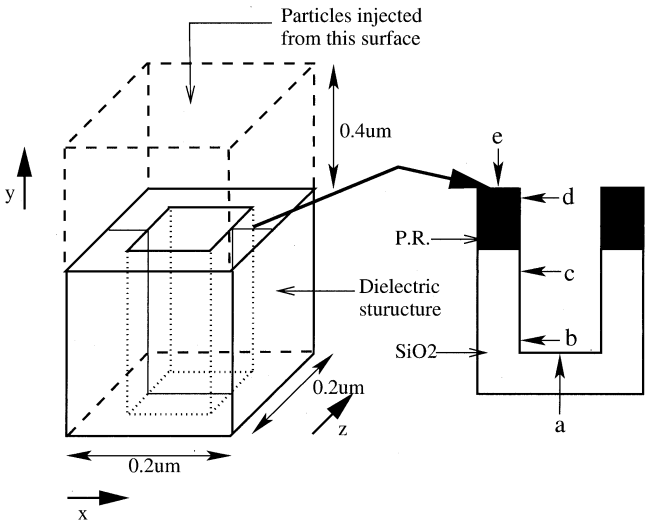

Fig. 2. Schematic of simulation domain (left), trench width is 0.1 μm, and xy plane dielectric structure with the special position form (a)-(e) (right).

back ($z = z_{\max}$), forth ($z = 0$), top ($y = y_{\max}$), and bottom ($y = 0$). The particles that are injected from the top of the simulation domain are accelerated by potential distribution. The calculation of the movement of particles is sustained until all injected particles are absorbed into dielectric structure or reflected by the high potential to the outside of the simulation domain. For the collisionless case considered here, the ionization and excitation are not taken into account, and the potential is kept constant. If there is no simulation particles in the simulation space, the potential and electric field can be computed by using the Laplace equation, $\nabla^2 V = 0$ with consideration of modified dielectric surface charge. The finite-differences method (FDM)

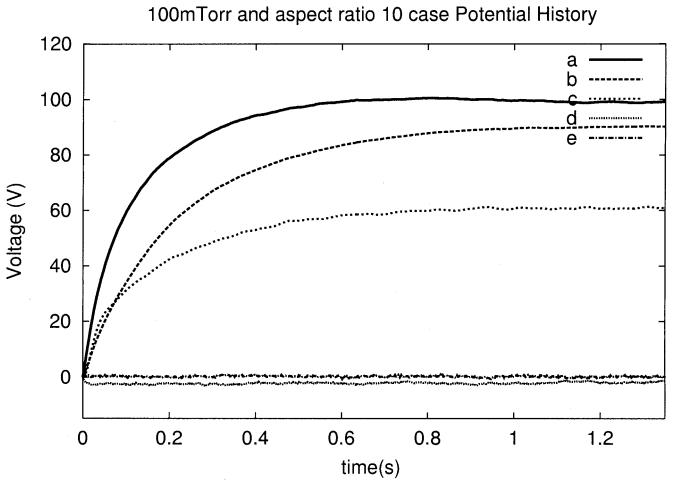

Fig. 3. Time trace of potential at each position described in Fig. 2. Pressure is 100 mtorr and aspect ratio is 10.

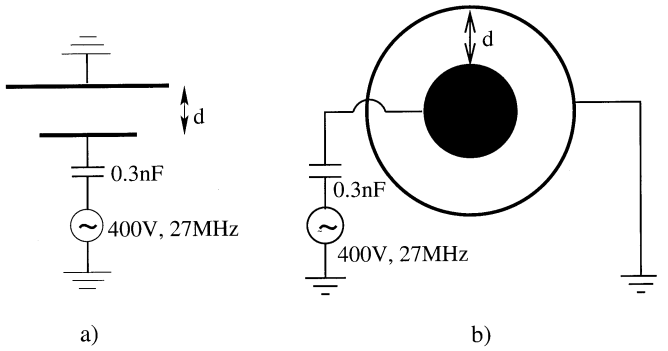

Fig. 4. Schematic of RF-CCP chamber with external circuit. (a) Conceptual schematic of real RF-CCP chamber. (b) Schematic of 1-D cylindrical simulation domain.

is employed, with the following boundary conditions: at the left, right, back and forth boundary, the Neumann boundary condition, $\nabla V = 0$ and the periodic boundary conditions, $V_{\text{left}} = V_{\text{right}}$, $V_{\text{back}} = V_{\text{forth}}$ are adopted, and at the top and bottom the Dirichlet boundary conditions, $V_{\text{top}} = 0$, $V_{\text{bottom}} = 0$ are used. Particles arriving at periodic boundary pass the boundary and ejected from opposite side periodic boundary. Particles reaching trench structure are absorbed, and there is no reflection and secondary electron emission. The details of calculation of potential and E-field are similar to conventional PIC methods [9], [10].

After hundreds or thousands of computational cycles, the potential of the entire simulation space goes to saturation because ion and electron fluxes are the same at the dielectric surface. The potential histories at the positions marked in Fig. 2 are traced in Fig. 3.

Using the PIC method, we can monitor not only the potential but also the data related with the movement of particles like the number of absorbed particles, energy, and incident angle at the surface structure. By using this data, many diagnostics can be obtained. The etch rate is a good example. We simply calculate the etch rate at each position on the structure and predict the trend of etching at the given structure. We consider ion-enhanced plasma etching, assuming that the wall of the structure is fully covered by active radicals so the etch rate is limited by the flux and velocity of incident ions. The deposition of passivation layer is not considered. The etch rate can be calculated as follows [7], [11], [12]:

$$\mathbf{ER} = A\left[V_i^{1/2} - V_{th}^{1/2}\right] \text{ when } \theta_i < 45^\circ \tag{1}$$

$$\mathbf{ER} = A\left[V_i^{1/2} - V_{th}^{1/2}\right] \frac{\cos\theta_i}{\cos 45^\circ} \text{ when } \theta_i > 45^\circ. \tag{2}$$

Here, V_i is the incident energy of a particle, V_{th} is the threshold potential which is set to 30 eV for SiO_2 etching.

III. Simulation Results and Discussions

A. RF-CCP Simulation and Results

The aim of the RF-CCP source simulation is to obtain the movement data of incident particles at the electrode. The schematic diagram of one-frequency RF-CCP chamber is presented in Fig. 4(a). The schematic diagram of one-dimensional (1-D) cylindrical simulation is presented in Fig. 4(b). We simulate 3 different pressure regimes of 10, 50 and 100 mtorr for pure Ar. The distance between two electrodes is modified to keep nearly the same flux to the electrode. Thus, the following distances and pressure have been considered 1.6 cm at 100 mtorr, 2.1 cm at 50 mtorr, and 3.2 cm at 10 mtorr. The 1-D cylindrical PIC code, XPDC1, has been used to obtain IAEDF and EAEDF [5]. The collisions and dynamics of electrons and ions are computed by using the PIC Monte Carlo collision (PIC-MCC) method. Since kinetic simulations using the PIC method can simply compute the motions of the collection of charged particles, the data related to movement of particles are easily obtained. In the CCP which consists of two plates, the 1-D simulation domain is close to the real chamber structure as the plate size is much larger compared to the distance between two plates. The cylindrical 1-D code can consider an unequal area electrode with negative self-bias voltage at a smaller electrode. The area ratio of two electrodes is 1:1.7. A 0.3-nF external capacitor is connected between the small electrode and RF voltage source whose amplitude is 400 V and frequency is 27 MHz. The large electrode is grounded, and no external capacitor is connected. The self bias voltage range varies from 75 to 186 V, according to the potential of RF voltage source.

Table I shows the plasma chamber conditions. The plasma density increases with the increase of plasma chamber pressure and the flux at each pressure is nearly the same. When the pressure is raised, the average energy of ions and electrons decreases. The frequent collisions at high pressure widen the average ion angle, however, the average electron angle is nearly the same. Fig. 5 shows the AEDF of ions and electrons at the electrode. As can be seen, the angle distribution of low-energy particles is wider than that of high-energy particles. Since the angle distribution is different for different energy, the particle movement information obtained by monitoring the angle distribution function (ADF) and the energy distribution function (EDF) separately can be the reason for an error factor. In general, high frequency (HF) low pressure CCP, the high- and low-energy peaks appear in the IEDF. However, in our simulation with the 27-MHz RF voltage source, double peaks do not appear because of the slow ion response to the quickly varying potential [13]–[16]. Instead of double peaks

TABLE I
PLASMA CHAMBER CONDITIONS

	Avg. ion energy (eV)	Avg. ion angle (°)	Avg. electron energy (eV)
10mTorr	189.48	4.80	6.24
50mTorr	103.48	9.39	4.51
100mTorr	73.29	9.91	3.59

	Avg. electron angle (°)	Flux at electrode ($m^{-2}s^{-1}$)	Plasma density (cm^{-3})
10mTorr	41.86	1.51×10^{19}	1.95×10^{10}
50mTorr	42.05	1.39×10^{19}	3.65×10^{10}
100mTorr	44.00	1.42×10^{19}	5.04×10^{10}

potential distribution, many ions are centered in the high-energy range. At the 10-mtorr pressure, high-energy and low-angle ions are dominant. On the other hand, for the 100-mtorr pressure discharge, low-energy and relatively high-angle ions are the main portion of the total number of incident ions at the electrode. For the 50-mtorr case, percentage of middle energy ions is higher than that of low or high energy. The difference, however, is not so much. Note, that the angle of high-energy ions is low in the high-pressure IAEDF. The results of the source simulation confirm the fact that high-energy and more anisotropic ions are principally observed at the low pressure. On the other hand, low-energy and less anisotropic ions are mainly monitored at high pressure. The movement difference between ions and electrons is reduced at high pressure because of the increase of ion incident angle. The IAEDF and EAEDF presented in Fig. 5 are used for the information of movement of the initially emitted particles at the top of charging simulation domain.

B. Charging Simulation and Result

In Fig. 2, the 3-D simulation domain is shown. Each length in the x and z directions for the rectangular simulation domain is 0.2 μm, and the length in y direction is 0.95 μm for aspect ratio 5 and 1.45 μm for aspect ratio 10. The inner width of the trench in the x and z direction is 0.1 μm, and the depth of the trench is 0.5 μm for aspect ratio 5 and 1 μm for aspect ratio 10. The etched material is SiO_2 covered with photo resist (PR). The thickness of PR is 0.3 μm for the aspect ratio 5 and 0.2 μm for the aspect ratio 10 because PR is also etched with SiO_2. The ions and electrons are emitted from the top region of the simulation domain. The distance between the top of PR and the top of the simulation domain is 0.4 μm.

Fig. 3 shows the time history of potential at the particular points indicated in Fig. 2. At the position (a), which is the center of trench bottom, the potential quickly increases at the initial stage of charge-up and then goes to saturation. At the initial charging period, only ions can arrive at the trench bottom, and most of electrons are piled up on the top sidewall owing to electron shading effect. During the potential increment, the electron flux at the trench bottom increases because electrons are attracted by high potential of the trench sole. This trend is similar for the positions (b) and (c) with different potential value for position (a). The potential at (d) is negative, but the absolute value is not so high. After about 1 s, the potential at each region goes to saturation. At the saturation period, the incident ion flux and the electron flux at the trench structure are same. The incident ion and electron fluxes at the position (a) marked in Fig. 2 are 0.78×10^{18} $m^{-2}s^{-1}$, 0.39×10^{19} $m^{-2}s^{-1}$ at the position (b), and 1.42×10^{19} $m^{-2}s^{-1}$ at the position (e).

Figs. 6 and 7 show the saturated potential distribution in the simulation domain (xy plane, $z = 0.1$ μm). Fig. 6 is the contour plot of the potential for the aspect ratio 5 case, and Fig. 7 is for the aspect ratio 10 case. In Fig. 6, the maximum charge-up potential is 220 V in the 10 mtorr, 94 V in the 50 mtorr, and 61 V in the 100 mtorr. The maximum charge-up voltage at the trench bottom is higher than the average incident ion energy of the 10-mtorr pressure case. At 10-mtorr pressure the incident particles are characterized by low-incident ion angle and high-electron temperature. The small ion incident angle increases the difference between ions and electrons. Since a stronger electric field is needed to draw high energetic and isotropic electrons to the trench bottom, large electron energy prevents the electrons from getting to the trench bottom. To attract high-energy electrons, a higher potential is required. Fig. 8 shows the effect of electron temperature on the charge-up potential distribution at the trench bottom. When constant energy and perfectly anisotropic ions are emitted with the same number of isotropic electrons, the saturated charging potential is varied according to the electron temperature. Three cases for average electron energies of 1.5, 3, and 6 eV with Maxwellian velocity distribution are represented in Fig. 8. The ion energy is 300 eV and the flux of ion and electron are 1.44×10^{19} $m^{-2}s^{-1}$ for each case. As can be seen, a higher saturated potential is generated as electron temperature increases. The potential distribution profile is also different. For 1.5 and 3 eV electron temperature cases, the potential of the central region is lower than that of the edge region. The potential difference between the two regions is more profound for the 1.5-eV case. For 6-eV electron temperature case, a higher potential is generated at the central region. The lower potential in the central region promotes the etching of the central region, and the higher potential of central region accelerates the etching of edge or sidewall regions. If the difference between the two regions is significant, PPID-like bowing and notching can occur. In any case, the low-ion angle and the high-electron temperature increase the charge-up potential.

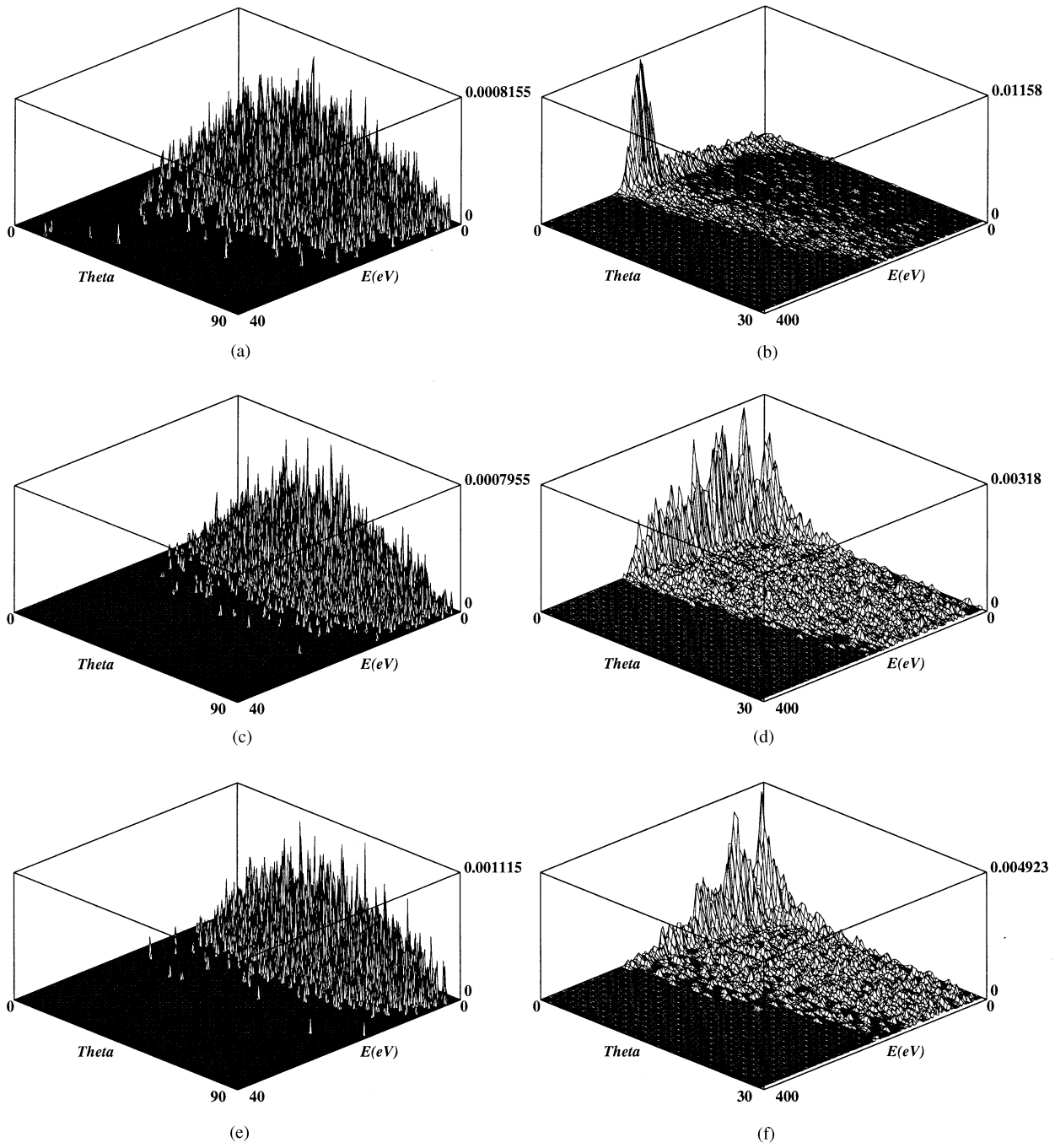

Fig. 5. AEDF at incident particles at the electrode with various pressure. (a) EAEDF at 10-mtorr pressure. (b) IAEDF at 10-mtorr pressure. (c) EAEDF at 50-mtorr pressure. (d) IAEDF at 50-mtorr pressure. (e) EAEDF at 100-mtorr pressure. (f) IAEDF of 100-mtorr pressure.

In Fig. 7, the potential distribution for the aspect ratio 10 case shows the similar results as in Fig. 6. However, the saturation potential is higher than that of the aspect ratio 5 case. The saturated potential at the trench bottom is higher than the average incident energy not only for 10-mtorr pressure case but also for 50- and 100-mtorr cases.

Using the saturated potential distribution, we calculate the etch rate. Due to the presence of many high-energy and low-angle ions, the etch rate for 10-mtorr pressure at the trench bottom is higher, and vertical etching is more available than for 50- and 100-mtorr pressure cases. Fig. 9 shows the normalized etch rate along the SiO_2 surface (from the left sidewall to the right sidewall). For each aspect ratio, the etch rate at all positions is normalized by the maximum etch rate. In Fig. 9(a), the etch rate for aspect ratio 3 case is shown. The depth of PR is 0.1 μm, and the etched depth of SiO_2 is 0.2 μm. The normalized etch rate of the trench bottom is presented at the position from 20 to 39, and the appearance of the sidewall etch rate is observed at other positions. Positions 0 and 58 is just below PR. In this case, the vertical thickness of PR is 0.1 and 0.2 μm for SiO_2 sidewall. The maximum saturated charge-up potential at the trench bottom is 186 V for the 10-mtorr case, 74 V for the 50-mtorr case, and 56 V for the 100-mtorr case. It is noted that the etch rate for 10- and 50-mtorr cases is

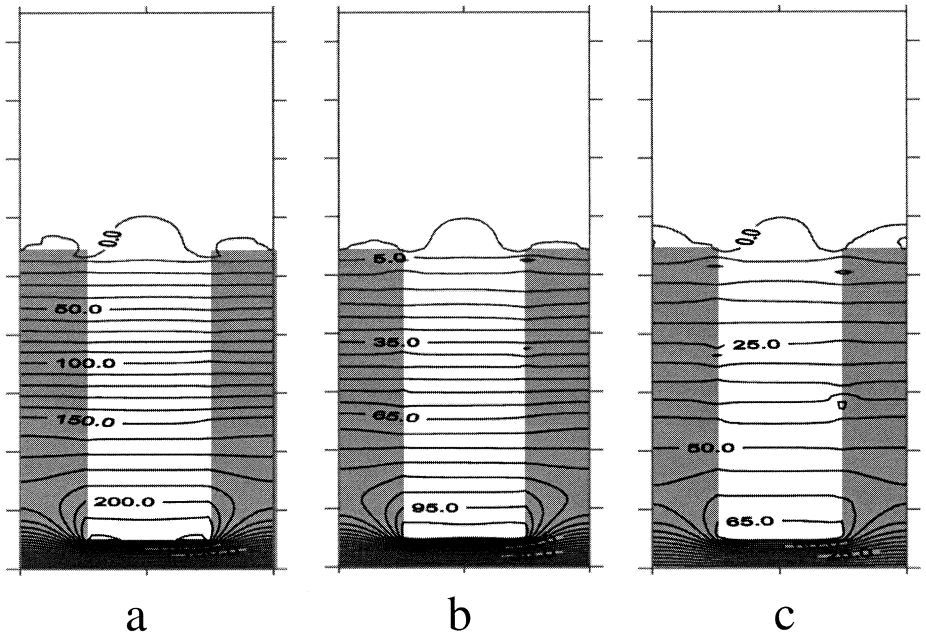

Fig. 6. Potential distribution contour in xy-plane at $z = 0.1$ μm when aspect ratio is 5. (a) 10 mtorr. (b) 50 mtorr. (c) 100 mtorr.

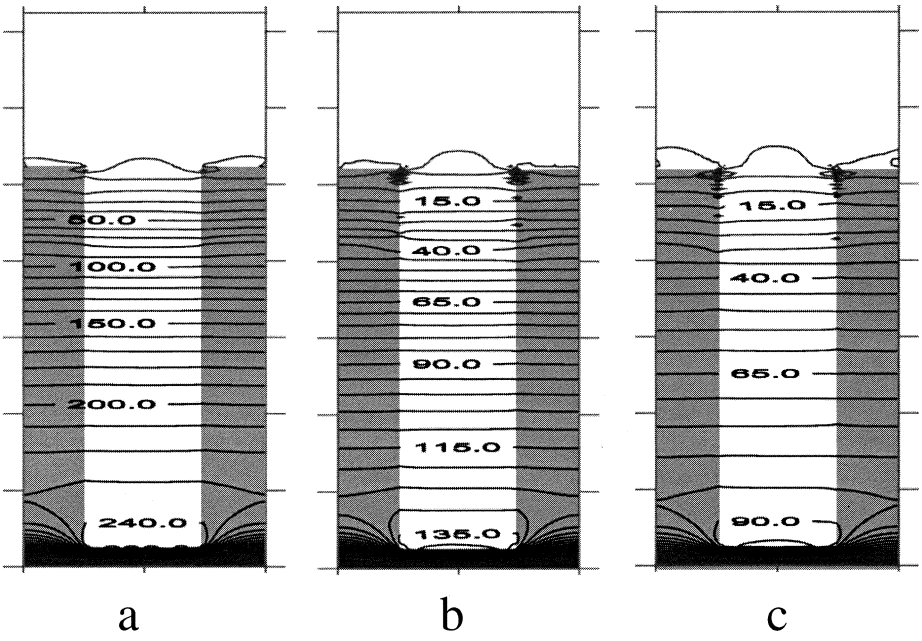

Fig. 7. Potential distribution contour in xy plane at $z = 0.1$ μm when aspect ratio is 5. (a) 10 mtorr. (b) 50 mtorr. (c) 100 mtorr.

high and the etch rate of the bottom region is much higher than that of the sidewall. Thus, for all the three cases, good vertical etching can be achieved. Though a higher average ion angle is found at high pressure, the main reason for the high-average angle is the large number of low-energy ions. Since ion-enhanced etching is assisted by high-energy ions, most of the low-energy and high-angle ions do not contribute to the sidewall etching. In Fig. 9(b), the etch rate for aspect ratio 5 case is presented. In this case, the vertical thickness of PR is 0.3 μm and 0.2 μm for SiO_2 sidewall. The etch rate for the 50-mtorr case is the highest of all three cases. The vertical etch is available for the all pressures. In Fig. 9(c), for the aspect ratio 10 case, the etch rate trend is similar to the aspect ratio 5 case, however, sidewall etch rate is not negligible. In this case, the vertical thickness of PR is 0.2 μm and 0.8 μm for SiO_2 sidewall. All the three pressure cases show a high etch rate of the sidewall, especially near the PR. This high etch rate of the sidewall top region causes an undercut effect which drives the structure under the PR. This phenomenon is the most profound for the 10 mtorr pressure case because the etch rate of the upper sidewall is nearly equal to that of the trench bottom. Thus, we can see that the etching characteristics for low-pressure conditions is good for the low-aspect ratio. However, as the aspect ratio increases, harmful etching features

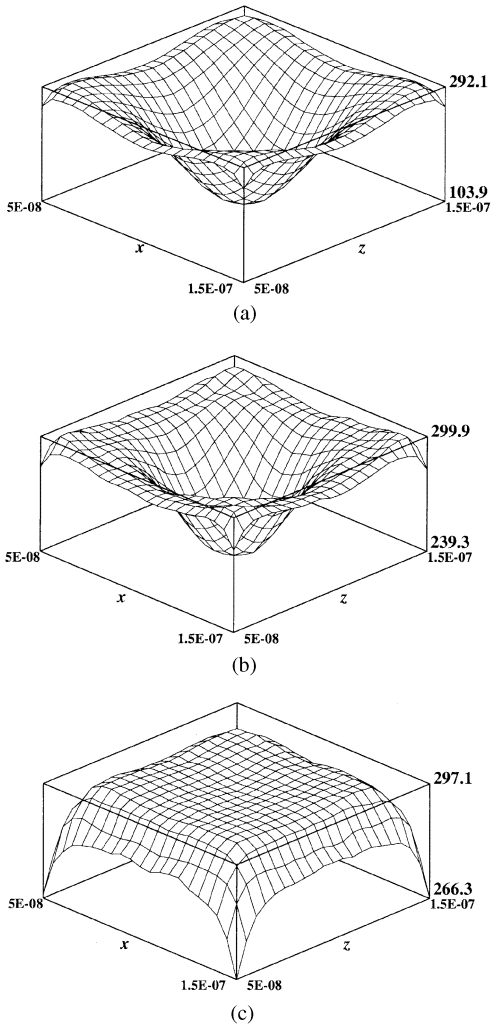

Fig. 8. Potential distribution of trench bottom in $z\,x$ plane with various electron temperature when ion energy is 300 eV. (a) $T_e = 1.5$ eV. (b) $T_e = 3$ eV. (c) $T_e = 6$ eV.

like the low etch rate and undercutting can appear. For medium or high pressure conditions, this phenomenon is less serious than for low pressure.

IV. Conclusion

We have presented an RF-plasma source simulation and 3-D charge-up simulation which can predict the trend of etching in micro SiO_2 structure. At first, we simulated RF-CCP for three different pressures: 10, 50, and 100 mtorr. At low pressures like 10 mtorr, high-energy and low-incident angle ions are abundant. On the other hand, at high pressure, there exist many ions with relatively low-energy and high-incident angles. Using the data of the particle movement obtained from the RF-CCP simulation, the charge-up potential is calculated. A higher potential is generated at the trench bottom when ion incident angle is low and the electron energy is high. Since low-angle and high-energy ions are abundant in the 10 mtorr pressure RF-CCP, the charge-up potential in the low pressure chamber is higher than that in the high pressure RF-CCPs like 50 or 100 mtorr. In general, the low-incident angle of ions is required for the vertical etching and this is correct for the low aspect ratio structure. However, when the charge-up effect is considered, low incident angles of ions

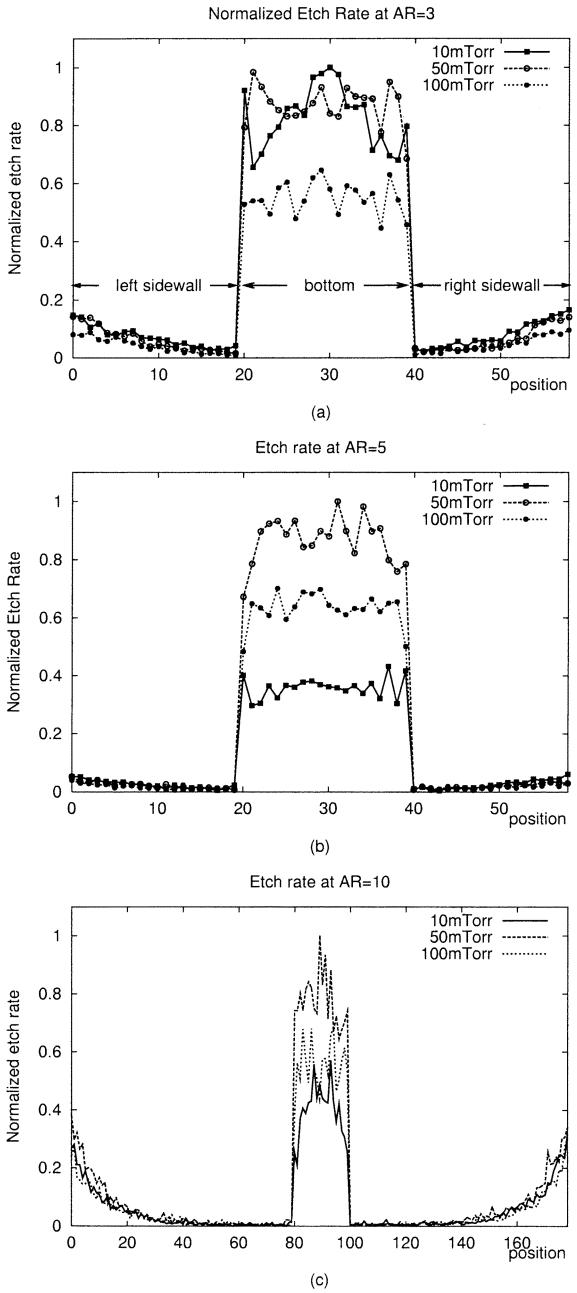

Fig. 9. Normalized etch rate along the wall of structure: (a) aspect ratio = 3, (b) aspect ratio = 5, and (c) aspect ratio = 10. The interval of each position number is 10 nm for sidewall, and 5 nm for bottom.

can be the reason for serious charge-up damage like notching or bowing at the high aspect ratio microstructure etching. In our research, the 50-mtorr pressure CCP chamber shows a noticeable reduction of charge-up potential because of the small angle difference between ions and electrons. Though the angle difference is also small for the 100 mtorr, the lack of high energy ions results in relatively low etch throughput. Eventually, both low energy with high-angle ions and high-energy ions are needed to reduce PPID, and these ions can be generated at proper pressure.

Acknowledgment

The authors would like to thank Dr. H. J. Lee for his working on code development.

REFERENCES

[1] K. Hashimoto, "Charge damage caused by electron shading effect," *Jpn. J. Appl. Phys.*, vol. 33, pp. 6013–6018, Oct. 1994.

[2] T. Nozawa, T. Kinoshita, T. Nishizuka, A. Narai, T. Inoue, and A. Nakaue, "The electron charging effects of plasma on notch profile defects," *Jpn. J. Appl. Phys.*, vol. 34, pp. 2107–2113, Apr. 1995.

[3] J. Matsui, K. Maeshige, and T. Makabe, "Effect of aspect ratio on topographic dependent charging in oxide etching," *J. Phys. D, Appl. Phys.*, vol. 34, pp. 2950–2955, Sept. 2001.

[4] H. J. Lee and J. P. Verboncoeur, "Simulation of a positive column discharge with a one-dimensional radial radiation transport coupled particle-in-cell model," *J. Appl. Phys.*, vol. 90, no. 10, pp. 4957–4965, Nov. 2001.

[5] J. P. Verboncoeur, M. V. Alves, V. Vahedi, and C. K. Birdsall, "Simulaneous potential and circuit solution for 1-D bounded plasma particles simulation codes," *J. Comput. Phys.*, vol. 104, pp. 321–328, Feb. 1993.

[6] T. Kinoshita, M. Hane, and J. P. McVittie, "Notching as an example of charging in uniform high density plasmas," *J. Vac. Sci. Technol. B*, vol. 14, no. 1, pp. 560–565, Jan/Feb. 1996.

[7] G. S. Hwang and K. P. Giapis, "On the origin of the notching effect during etching in uniform high density plasmas," *J. Vac. Sci. Technol. B*, vol. 15, no. 1, pp. 70–87, Jan/Feb. 1997.

[8] J. Matsui, N. Nakano, Z. L. Petrovic, and T. Makabe, "The effect of topographical local charging on the etching of deep-submicron structures in SiO_2 as a function of aspect ratio," *Appl. Phys. Lett.*, vol. 78, pp. 883–885, Feb. 2001.

[9] C. K. Birdsall and A. B. Langdon, *Plasma Physics Via Computer Simulation*. Bristol, U.K.: Hilger, 1991, pp. 7–80.

[10] C. K. Birdsall, "Particle-in-cell charged-particle simulations, plus monte carlo collisions with neutral atoms, PIC-MCC," *IEEE Trans. Plasma Sci.*, vol. 19, pp. 65–85, Apr. 1991.

[11] N. R. Rueger, J. J. Beulens, M. Schaepkens, M. F. Doemiling, J. M. Mirza, T. E. F. M. Standaert, and G. S. Oehrlein, "Role of steady state fluorocarbon films in the etching of silicon dioxide using CHF_3 in an inductively coupled plasma reactor," *J. Vac. Sci. Technol. A*, vol. 15, no. 4, pp. 1881–1889, Jul/Aug. 1997.

[12] J. P. Chang and H. H. Sawin, "Kinetic study of low energy ion-enhanced polysilicon etching using Cl, Cl_2, and Cl^+ beam scattering," *J. Vac. Sci. Technol. A*, vol. 15, no. 3, pp. 610–615, May/Jun. 1997.

[13] H. H. Doh, C. K. Yeon, and K. W. Whang, "Effects of bias frequency on reactive ion etching lag in an electron cyclotron resonance plasma etching system," *J. Vac. Sci. Technol. A*, vol. 15, pp. 664–667, May/June 1997.

[14] V. Vahedi, C. K. Birdsall, and M. A. Lieberman, "Verification of frequency scaling laws for capacitive radio-frequency discharges using two-dimensional simulations," *Phys. Fluids B*, vol. 5, pp. 2719–2729, July 1993.

[15] Z. L. Dai, Y. N. Wang, and T. C. Ma, "Spatiotemporal characteristics of the collisionless rf sheath and the ion energy distributions arriving at rf-biased electrodes," *Phys. Rev. E, Stat. Phys. Plasmas Fluids Relat. Interdiscip. Top.*, vol. 65, pp. 036403.1–036403.7, Feb. 2002.

[16] M. Surendra and D. B. Graves, "Particle simulations of radio-frequency glow discharges," *IEEE Trans. Plasma Sci.*, vol. 19, pp. 144–157, Apr. 1991.

Hye Sang Park was born in Daegu, South Korea, in 1978. He received the B.S. and M.S. degrees in electronic and electrical engineering from the Pohang University of Science and Technology, Pohang, South Korea, in 2001 and 2003, respectively.

He is currently with Samsung Electronics Company, Ltd., Hwasung, South Korea. His current research interests include theory and simulations of plasma etching and plasma process induced damage.

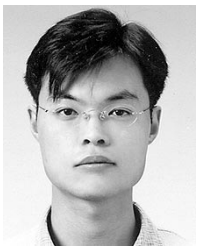

Sung Jin Kim was born in Jinhae, South Korea, in 1974. He received the B.S. degree in electronic and electrical engineering from Kyungpook National University, Kyungpook, South Korea, in 2000 and the M.S. degree in electronic and electrical engineering from the Pohang University of Science and Technology (POSTECH), Pohang, South Korea, in 2002. He is currently working toward the Ph.D. degree at POSTECH.

His research interests include theory and (PPID) and neutral beam etching process.

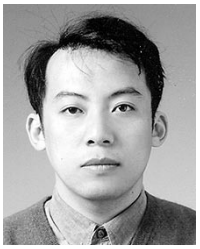

Yan Qing Wu was born in ShanDong, China, in 1968. He received the B.S. degree from Fudan University, Shanghai, China, in 1992 and the Ph.D. degree from Shanghai Institute of Optics and Fine Mechanics, Chinese Academy of Sciences, Shanghai, China, in 2000.

He is currently working as a Postdoctoral Researcher at the Pohang University of Science and Technology, Pohang, South Korea. His current research interests include theory and simulation of plasma process induced damage and RF capacitively coupled discharge.

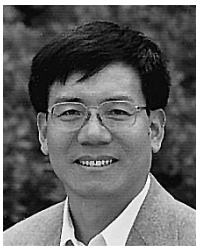

Jae Koo Lee (M'83) received the Ph.D. degree from the University of California, Berkeley, in 1979.

From 1979 to 1989, he was a Senior (later a Staff) Scientist on tokamak theory with General Atomics, San Diego, CA. He is currently a Professor in the Department of Electronic and Electrical Engineering, Pohang University of Science and Technology, Pohang, South Korea. He is currently on the Editorial Board of *Plasma Source and Science and Technology*. His research interests include the theory and simulation of low-temperature basic/processing plasmas, fusion plasmas, and free-electron lasers.

Dr. Lee is the past Chair of Division of Plasma Physics of Korean Physical Society.